Flexible Superhydrophobic Metal-based Carbon Nanotube Membrane for Electrochemically Enhanced Water Treatment

Yiran Si[a], Chunyi Sun[a], Dongfeng Li[b], Fenglin Yang[a], Chuyang Y. Tang[c], Xie Quan[a], Yingchao Dong[a], Michael D. Guiver[d*]*

[a] Key Laboratory of Industrial Ecology and Environmental Engineering (Ministry of Education, MOE), School of Environmental Science and Technology, Dalian University of Technology, Dalian 116024, China

[b] School of Science, Harbin Institute of Technology, Shenzhen 518055, China

[c] Department of Civil Engineering, The University of Hong Kong, Pokfulam, Hong Kong S.A.R., China

[d] Key Laboratory of Engines, and Collaborative Innovation Center of Chemical Science and Engineering (Tianjin), Tianjin University, Tianjin 300072, China

Note: Yiran Si and Chunyi Sun made equal contributions to this work.

***Corresponding authors**:*

Prof. Michael D. Guiver

State Key Laboratory of Engines, and Collaborative Innovation Center of Chemical Science and Engineering (Tianjin), Tianjin University, Tianjin 300072, China

Tel: +86-158-22869113 E-mail: guiver@tju.edu.cn

Prof. Yingchao Dong

Key Laboratory of Industrial Ecology and Environmental Engineering (Ministry of Education, MOE), School of Environmental Science and Technology, Dalian University of Technology, Dalian 116024, China

Tel: +86-411-84706328 E-mail: ycdong@dlut.edu.cn

25

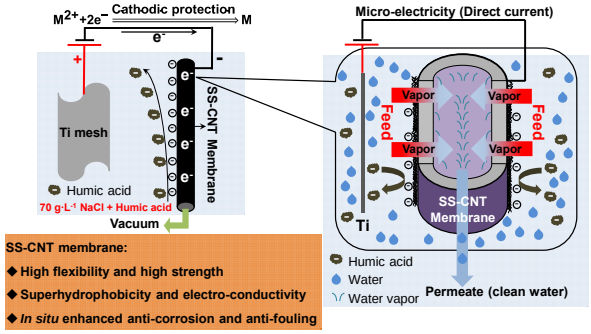
M2+ +2e− Cathodic protection M
e−
+
−
Ti mesh
SS-CNT Membrane
Humic acid
70 g·L-1 NaCl + Humic acid
Vacuum
Micro-electricity (Direct current)
Vapor
Vapor
Vapor
Vapor
Feed
Feed
SS-CNT Membrane
Ti
Humic acid
Water
Water vapor
Permeate (clean water)
SS-CNT membrane:
◆ High flexibility and high strength
◆ Superhydrophobicity and electro-conductivity
◆ In situ enhanced anti-corrosion and anti-fouling

26

ABSTRACT

Treatment of highly saline wastewaters via conventional technology is a key challenging issue, which calls for efficient desalination membranes featuring high flux and rejection, low fouling and excellent stability. Herein, we report a high-strength and flexible electro-conductive stainless steel-carbon nanotube (SS-CNT) membrane, exhibiting significantly enhanced anti-corrosion and anti-fouling ability via a micro-electrical field-coupling strategy during membrane distillation. The membrane substrates exhibited excellent mechanical strength (244.2±9.8 MPa) and ductility, thereby overcoming the critical bottleneck of brittleness of traditional inorganic membranes. By employing a simple surface activation followed by self-catalyzed chemical vapor deposition, CNT was grown *in situ* on SS substrates via a tip-growth mechanism to finally form robust superhydrophobic SS-CNT membrane. To address the challenging issues of significant corrosion and fouling, by using a negative polarization micro-electrical field-coupling strategy, simultaneously enhanced anti-fouling and anti-corrosion performance was realized for treatment of organic high salinity waters while exhibiting stable high flux and rejection via an electrostatic repulsion and electron supply mechanism. This application-oriented rational design protocol can be potentially used to extend toward high performance composite membranes derived from other electro-conductive metal substrates functionally decorated with CNT network and to other applications in water treatment.

INTRODUCTION

Membrane-based desalination is an effective way to mitigate the global challenge of water scarcity by purifying unconventional sources such as seawater, brackish water, or wastewaters to augment fresh water supplies.[1-3] Recently, membrane distillation (MD) has been broadly explored as a competitive emerging technology against other conventional methods such as reverse osmosis or electrodialysis, especially for challenging desalination applications.[4,5] MD offers promising advantages, such as excellent separation efficiency, excellent tolerance to high salinity, ultra-high salt enrichment and potential opportunities for resource and energy extraction.[6-8] By using low-grade waste heat or emerging heat resources such as solar and joule heating,[9-11] MD can be highly attractive in terms of lower energy cost, particularly for more challenging feedwaters (e.g., high salinity brines).

Existing MD membranes generally involve hydrophobic polymeric membranes and hydrophobically-modified inorganic membranes,[12-14] where surface hydrophobicity is effectively imparted via organic material-based surface grafting. Nevertheless, these two membrane types usually suffer from insufficient long-term stability, leading to undesirable issues such as wetting, fouling, and loss of flux and rejection under harsh operating environments.[15-17] In recent years, some efforts have been made to focus on developing advanced polymer-based membranes with novel inorganic nanomaterials such as silicon dioxide (SiO_2) or ZnO, which effectively enhanced mechanical properties and surface hydrophobicity to fulfill the potentials of MD process.[18,19] Although inorganic ceramic membranes can offer outstanding thermal and chemical

stabilities in harsh desalination applications,[20-23] their brittleness and poor processability greatly limit their practical applications. Beyond conventional MD application, high-strength MD membranes have a great potential especially in novel high-pressure MD processes such as thermal osmosis energy conversion process and PRO-MD coupled process.[9,24] In contrast, metal-based membranes, e.g., made from stainless steel (SS) powders, are mechanically stronger and more flexible, which makes them ideal candidates to fully address these mechanical issues.[25,26] Nevertheless, SS membranes can be prone to membrane fouling and corrosion, which needs to be systematically addressed to allow their wide-spectrum applications.[25,27] In addition, more cost-effective rational design strategies for preparing superhydrophobic SS membranes need to be further developed.

Herein, we report a mechanically strong and flexible superhydrophobic SS-metal-based carbon nanotube membrane featuring promising anti-fouling and anti-corrosion functions for electrochemically enhanced water treatment. A novel method is proposed to prepare a superhydrophobic SS hollow fiber (SSHF) membrane through *in situ* growth of carbon nanotubes (CNTs). By taking advantage of self-catalysis by SS during chemical vapor deposition (CVD), we prepared a superhydrophobic network layer of CNT using a simple surface activation, obviating the need for external catalyst addition (Figure S1). The resulting membrane was robust, mechanically stronger and flexible. We further take advantage of the high electro-conductivity of both SS and CNT to simultaneously enhance anti-fouling and anti-corrosion performance for treating high salinity waters containing organic foulant (humic acid). Specifically, in this novel

protocol, we demonstrate that the application of a negative polarization micro-electric field is able to maintain stable high flux and solute rejection. Our study offers a simple, yet highly effective approach for rational design of stable and high-performance desalination membranes, featuring multi-functionality under electrochemically *in situ* enhanced membrane separation process.

MATERIALS AND METHODS

Materials. 316L stainless steel powder (SS, D_{50} = 10.5 μm (Figure S2), Antai Technology Co., Ltd., USA), polyethersulfone (PES, Bei-Shi-De Synthetic Plastics Company, China) and N-methyl-2-pyrrolidone (NMP, Sinopharm Chemical Reagent Co., Ltd., China) were used as raw material, polymeric binder and solvent, respectively to form a suspension. Polyvinylpyrrolidone (PVP, Sinopharm Chemical Reagent Co., Ltd., China) was then used to enhance the viscosity of the suspension.[28,29] The SS power and PES were fully dried at 60 °C for 48 h, while all other chemicals were used without further treatment. All the gases (ethylene, hydrogen and nitrogen, purity ≥ 99.999%) were purchased from Dalian Guanghui Gas Co., Ltd, China.

Preparation of SS-CNT membrane. A dry-wetting spinning technique involving immersion-induced phase inversion and dry-sintering process was applied to prepare SSHF membrane substrates (Supporting Information S2).[30,31]

The SSHF membrane substrates were soaked in water and then oxidized at 60 ℃ for more than 48 h in order to destroy their surface passive layers. Subsequently, *in situ* reduction was carried out at 700 °C for 70 min in H_2 at a flow rate of 40 mL·min^{-1} to

activate surface metal catalysis. A mixture of hydrogen and ethylene gases at a flow rate of 40 $mL \cdot min^{-1}$ was used during CVD, where the final reaction temperature was fixed at 700 ℃ for 1 h, leading to *in situ* growth of CNT on/inside SS substrates, to form SS-CNT membranes. After CVD reaction, hydrogen gas at a flow rate of 20 $mL \cdot min^{-1}$ was used to cool the reactor to room temperature (25 °C).

Membrane Characterization. Electrochemical impedance spectroscopy (EIS) of SSHF membrane substrate was performed in an electrochemical workstation (CHI660D, Shanghai Chenhua Company, China). The microstructure and surface morphology of the membranes were observed using a scanning electron microscope (SEM, QUANTA 450, American FEI Company, USA) equipped with energy dispersive spectrometer (EDS) analysis. Static water contact angle measurements were determined using an optical contact angle and interface tension meter (KINO SL 200KB, Corona Inc., USA). The crystal phases were characterized through an X-ray diffraction device (XRD, D/Max 2400, Japanese Institute of Neo-Confucianism) with a Cu Kα radiation source in the 2θ range of 5–80°. Surface chemical characterization was carried out by X-ray photoelectron spectroscopy (XPS, ESCALAB XI+, Thermo Company, Britain). The structure of CNTs was observed by high-resolution transmission electron microscope (HRTEM, JEOL 2010, Japan) at an accelerating voltage of 200 kV. The iron ion contents per unit membrane area were measured for the oxidized SS-CNT membrane surfaces under different voltages (+2 V, 0 V, -2 V) after 6 h operation by Inductively Coupled Plasma (ICP, Optima2000DV, Perkin Elmer Enterprise Management Co., Ltd, USA). Other characterization techniques, such as mechanical

strength, nitrogen performance, and pure water flux of SSHF membrane substrate are described in Supporting Information S2.2.

Membrane distillation performance tests. The vacuum membrane distillation (VMD) performance was evaluated in a laboratory-made VMD cross-flow test unit using simulated seawater (35 $g \cdot L^{-1}$ NaCl), high salinity water (70 $g \cdot L^{-1}$ NaCl), or high salinity water with organics (70 $g \cdot L^{-1}$ NaCl and 30 $mg \cdot L^{-1}$ humic acid) as the feed solutions. Feed solutions were maintained at 75 °C and were circulated using a peristaltic pump (60 rpm), while the permeate vapor was condensed via an ice-water bath (0 °C) under vacuum (-0.03 MPa). The mass and conductivity of permeate water were measured at a time interval of 1 h. The permeate flux (J, $L \cdot m^{-2} \cdot h^{-1}$) of produced water, and the salt rejection (R) can be calculated by the following equations:[17]

$$J = \frac{\Delta m}{A \cdot \rho \cdot \Delta t} \quad (1)$$

$$R = \left(1 - \frac{C_P}{C_f}\right) \times 100\% \quad (2)$$

where Δm (kg) is the weight of the permeate solution at a given time Δt (h), A (m^2) is the effective area of the membrane, and ρ is the water density (0.9982 $kg \cdot L^{-1}$, 20 °C). C_f and C_p are the conductivities ($mS \cdot cm^{-1}$) of the feed and permeate solutions, respectively.

RESULTS AND DISCUSSION

Mechanical and Electrical Properties of Substrates

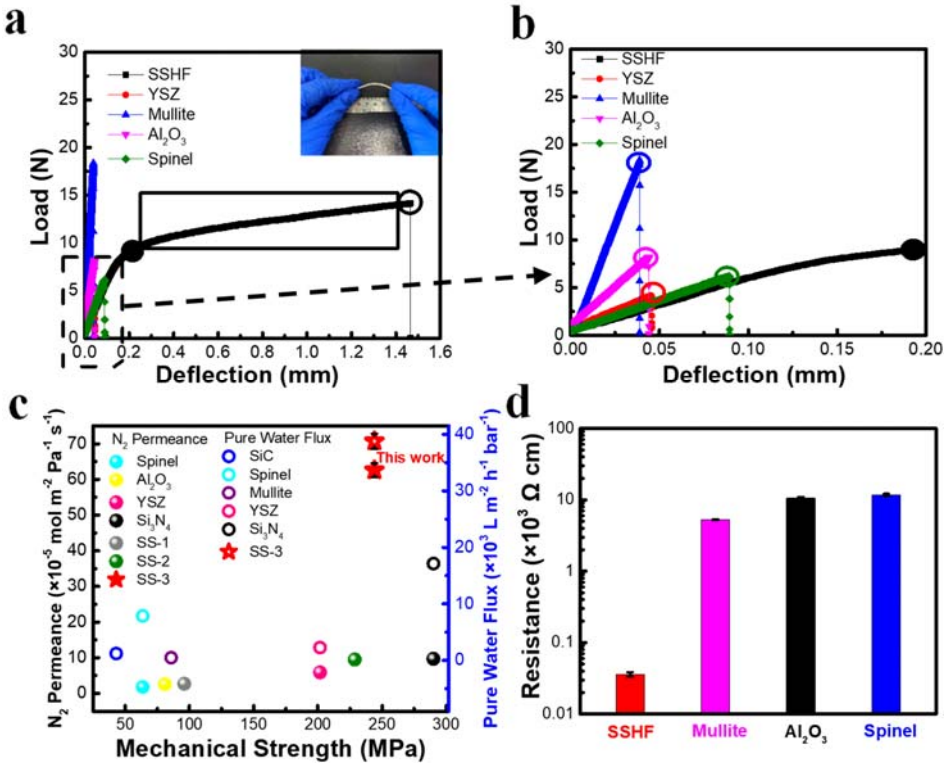

Figure 1. (a, b) Comparisons of bending fracture behavior between SSHF membrane substrates and ceramic membranes (Dashed line box: elastic deformation zone; solid line box: plastic deformation zone; solid circle: yield point; hollow circle: breaking point.). (c) Comparison in nitrogen (N_2) permeance (solid circle), pure water flux (hollow circle) with mechanical strength between SS membrane substrates (this study: SS-3; other studies: SS-1,[32] SS-2[31]) and existing ceramic membranes (spinel,[17] alumina (Al_2O_3),[33] yttria stabilized zirconia (YSZ),[34] silicon carbide (SiC),[35] Si_3N_4[36] and mullite[37]). (d) Comparison in electrical resistance of the SSHF membrane substrate (1050 °C) in this work and other ceramic membranes (Al_2O_3, mullite, spinel[17,37]).

Different from conventional brittle inorganic ceramic membranes, the SSHF membrane substrate exhibited a nonlinear load-deflection response due to its excellent metallic ductility (Figure 1a). It is noted that ceramic membranes have the same load-deflection curve geometries as the tested SSHF membrane substrate in the elastic

deformation zone (Figure 1b). Interestingly, however, unlike ceramic membranes having only an elastic deformation zone followed by failure, the bending fracture behavior of SSHF membrane substrate can be divided into two zones: elastic deformation and plastic deformation. This much better ductile behavior allows it to accommodate a maximum deflection of nearly 1.5 mm, showing 1-2 orders of magnitude improvement over conventional ceramic membranes (Figure 1b), indicating much better fracture tolerance and flexibility than ceramic membranes. Moreover, in spite of being sintered at a lower temperature of 1050 °C (compared to 1400-1700 °C that is typically used for ceramic membranes), the SS membrane substrate had higher bending strength (244.2±9.8 MPa) and fracture energy (447±71 KJ/m^3), outperforming many existing ceramic and SS membranes (except for Si_3N_4 membrane, see Figure 1c).[36] These mechanical properties of the SSHF membrane substrate (excellent mechanical strength and high flexibility) are beneficial for membrane module assembly. More robust flexible SS-based membranes can potentially address the challenging issues of membrane damage especially in practical industrial operation processes usually involving high pressure and vigorous vibration, where hollow fiber ceramic membranes cannot perform well due to their inherent brittleness and insufficient flexibility.[25,37-39] In addition, SSHF membrane substrate also exhibited better N_2 permeance and pure water flux than ceramic counterparts such as spinel, Al_2O_3, YSZ, SiC and mullite,[17,33-35,37] and other SS membrane substrates[31,32] (Figure 1c). Its electro-resistance (~ 35.9 Ω cm, see Figure 1d) was 2-3 orders of magnitude lower compared with other ceramic membranes (Al_2O_3, mullite, spinel),[17,37] allowing its coupling with

electrochemical methods to achieve enhanced MD performance (see Section "Electrochemically Enhanced Anti-fouling and Anti-corrosion Performance").

In Situ Growth of Carbon Nanotubes

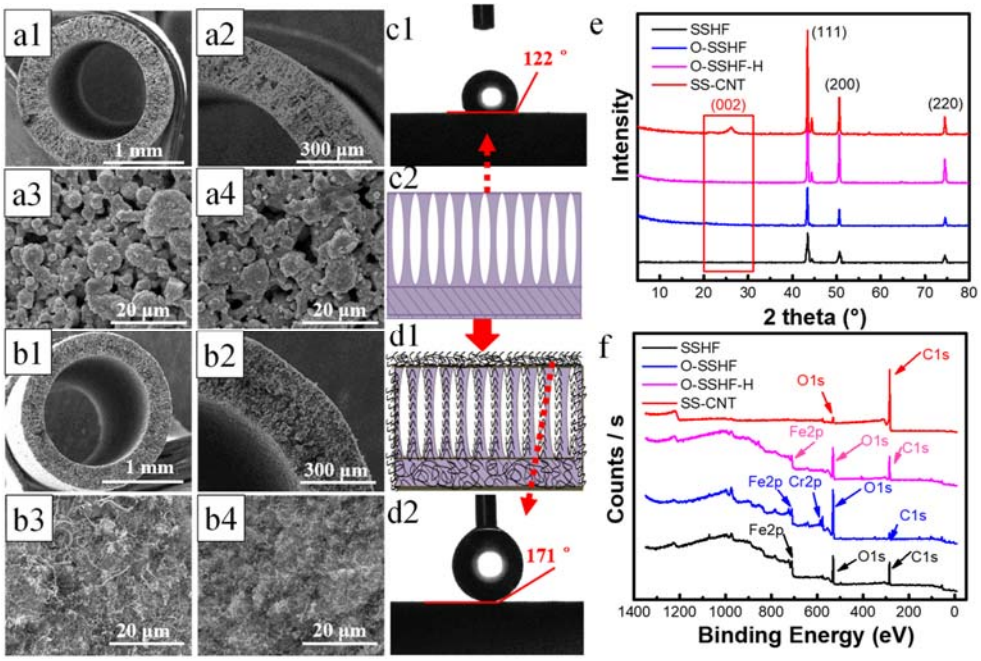

Figure 2. Cross-sectional SEM images (a1, b1), locally enlarged cross-sectional SEM images (a2, b2), inner surface SEM images (a3, b3), and outer surface SEM images (a4, b4) of SSHF substrate (a) and SS-CNT membrane (b); water contact angles measured at room temperature (~25 ℃) on the membrane surface of SSHF substrate (c1) and SS-CNT membrane (d2); simplified half structural models of cross-sectional structures of SSHF substrate (c2) and SS-CNT membrane (d1) (light purple color, SSHF substrate; black color, CNT); and XRD patterns (e) and XPS spectra (f) of raw SSHF, SSHF membrane substrate after oxidation (O-SSHF), O-SSHF membrane substrate after reduction (O-SSHF-H) and SS-CNT membrane fabricated via CVD without additional nano-catalyst.

Since the SS powders inherently contain Ni and Fe elements,[40,41] a self-catalyzed chemical vapor deposition, after a simple surface activation, was used to grow CNTs *in situ* on the SS substrate without external catalyst addition. An asymmetric sandwich structure with porous inner/outer surfaces is observed for SSHF substrate (Figures 2a1-2a4), exhibiting a hydrophobic nature (water contact angle ~122°, Figure 2c1).

Different from traditional membrane structures, this highly porous asymmetric structure, combined with superhydrophobic and superporous CNT surface, could effectively reduce conductive heat loss across the membrane.[38] Thermal cracking of ethylene via self-catalyzed CVD led to the formation of a superporous CNT layer (Figures 2b3 and 2b4). Simplified half-structural models of cross-sectional structures of SSHF substrate and SS-CNT membrane are illustrated in Figures 2c2 and 2d1. For SS-CNT membrane, the average pore size is 0.57 μm, while the liquid entry pressure (LEP) is 0.4 bar (Figure S4). The *in situ* growth of the CNT layer increased the water contact angle of the membrane from ~122° (hydrophobicity) to ~171° (superhydrophobicity) (Figure 2d2). Such an excellent superhydrophobicity characteristic is beneficial for MD (Table S4), because it inhibits pore penetration and wetting by water, while enabling rapid vapor transport through the membrane pores.[16,42]

Revealing *in situ* growth mechanism of CNT is important to gain a deep understanding on both the catalytic function of true active components and CNT growth model on SS substrate surface.[43] Growth of CNTs to form SS-CNT membrane involves two key stages (Figure 3c):

(1) surface activation of catalytic sites via a simple oxidation and reduction process.[44] Due to the presence of thin passive surface layers, the sintered SS substrates are inert to gaseous hydrocarbons.[41] The water-soaked SSHF membrane substrates were heated at 60 °C for 48 h to sufficiently oxidize their passive layers into oxide layers on SSHF substrate surfaces, which is confirmed by a stronger oxygen signal in the XPS spectra (Figure 2f). Subsequent reduction treatment in H_2 reduced surface metal oxides (NiO and Fe_2O_3) into active metallic catalysts.[45] The oxidation and reduction process did not

introduce new impurity phases, which is fully confirmed by the membranes having a typical austenitic steel structure as well as the original SSHF substrate (Figure 2e). Although it is hard to identify metallic elements via XRD, zero-valence state active metallic catalysts (Ni and Fe) can be confirmed by TEM (Figures S5b2-d2).

(2) *In situ* nucleation and growth of CNT via self-catalyzed CVD.[46,47] A dominant reflection (002), corresponding to carbon element is observed for SS-CNT membrane (Figure 2e). TEM results clearly reveal that the resulting nanocarbon materials were hollow, with the CNTs having open ends (red arrow) rather than solid carbon nanofibers (Figure 3a). An interplanar d-spacing of ~0.34 nm is observed between two tube walls, which is characteristic of (002) reflections of CNTs (Figure 3a inset).[48] CNTs containing metallic Ni nano-catalyst on the tip was confirmed, indicating a tip growth model mechanism is dominant (Figure 3b).

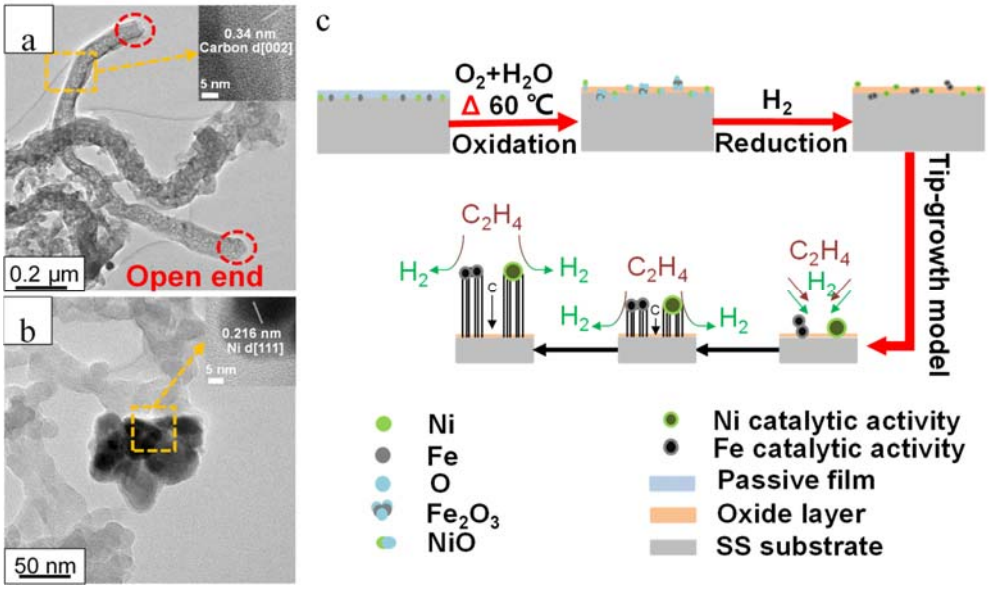

Figure 3. (a) TEM image of CNTs with open end. (b) TEM image of CNTs with catalyst particles on the tip. (c) *In situ* growth mechanism of CNTs on a SSHF membrane substrate based on a strong interaction between SSHF membrane substrate and its inherent Ni and Fe catalyst via a tip-growth

model.

Electrochemically Enhanced Anti-fouling and Anti-corrosion Performance

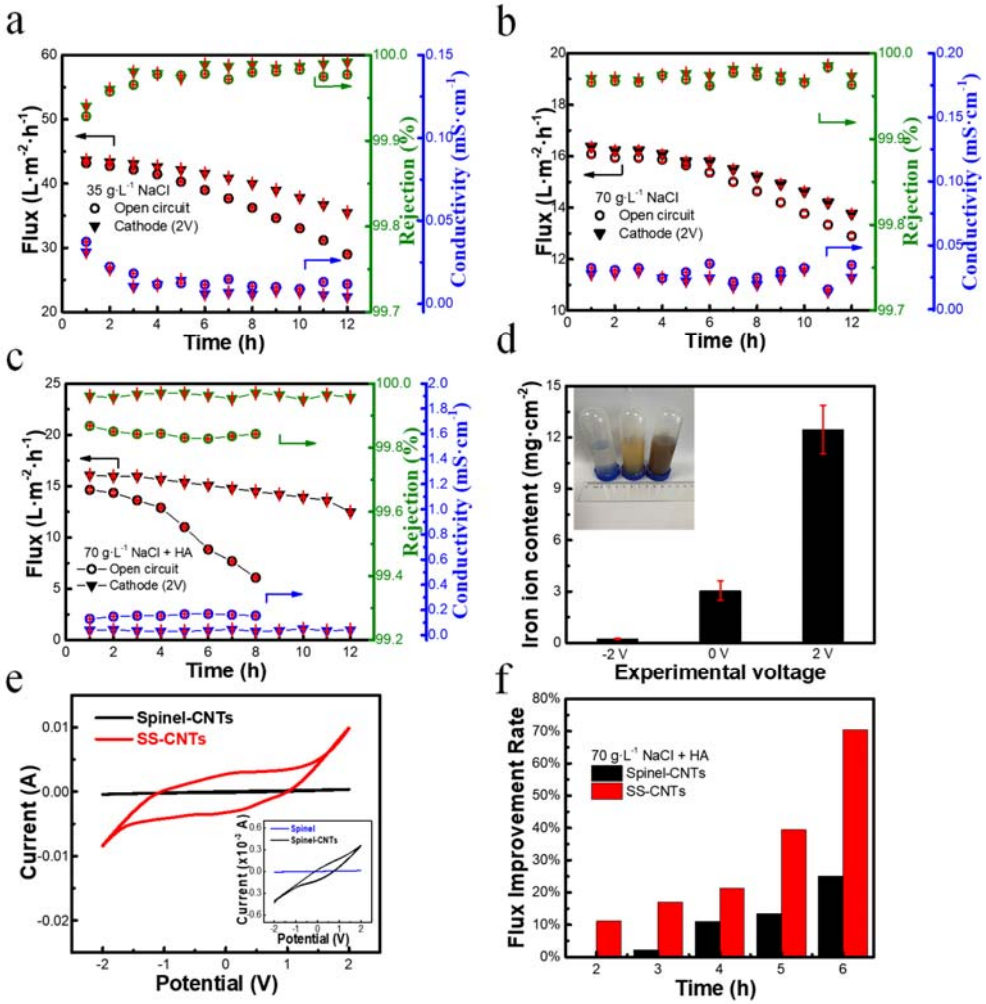

Figure 4. VMD performance (flux, salt rejection and distillate conductivity) of the SS–CNT membranes for the treatment of high salinity water under open circuit and negative polarization ((a) 35 g·L^{-1} NaCl, (b) 70 g·L^{-1} NaCl, (c) 70 g·L^{-1} NaCl + 30 mg·L^{-1} HA). (d) Comparison in the iron ion content of the oxidized surface per unit membrane area of the SS-CNT membranes under different voltages after 6 h operation for treatment of 70 g·L^{-1} NaCl feed solution (the inset shows the photographs of the ferric oxide suspensions for corrosion oxidation of SS-CNT membrane surfaces under different voltages (-2 V, left; 0 V, middle; +2 V, right) after 6 h operation). (e) Comparison in CV curves of SS-CNT membrane and spinel-CNT membrane (the inset shows the CV curves of spinel-CNT membrane and spinel substrate[17]). (f) Comparison in flux improvement

258 percent under negative polarization during 6 h operation of SS-CNT membrane and spinel-CNT
259 membrane for treatment of organic high salinity waters (70 $g \cdot L^{-1}$ NaCl and 30 $mg \cdot L^{-1}$ HA).

260 Membrane fouling and corrosion are among the key challenges for membrane
261 distillation treatment of high salinity water when using metallic-based membranes. In
262 order to address this issue, desalination performance was systematically investigated in
263 vacuum membrane distillation process under a micro-electrical field-assisted strategy
264 (Figure 4). For simulated seawater (35 $g \cdot L^{-1}$ NaCl), the water flux of SS-CNT
265 membrane decreased from 43.2 to 29.0 $L \cdot m^{-2} \cdot h^{-1}$, while salt rejection was maintained
266 at high level (above ~99.9%) during 12 h operation at open circuit (i.e., without micro-
267 electrical field assistance) (Figure 4a), due to membrane fouling and corrosion. In
268 comparison, a micro-electrical field-assisted MD system was exploited to efficiently
269 achieve less flux loss and high salt rejection, where the SS-CNT membrane was applied
270 as cathode under at -2.0 V negative polarization (Figure 4a). An increase in salt
271 concentration from 35 to 70 $g \cdot L^{-1}$ resulted in a decrease in water flux (Figure 4b) with
272 operating time under two cases (open circuit and negative polarization), while
273 maintaining high salt rejection (above ~99.9%). Similarly, under negative polarization
274 (-2.0 V), the SS-CNT membrane presented a higher water flux (13.8 $L \cdot m^{-2} \cdot h^{-1}$) after 12
275 h operation (Figure 4b) than that under open circuit. However, when applied as anode
276 at +2.0 V under positive polarization, the SS-CNT membrane underwent significant
277 corrosion, resulting in rapid wetting and without salt rejection, even at less than 1 h
278 operation. After 6 h VMD operation, higher Fe content under positive polarization was
279 confirmed than at open circuit and negative polarization by SEM-EDS Fe element
280 mapping analysis (Figure S6). When using high salinity water with organics (NaCl 70

281 g·L^{-1}, HA 30 mg·L^{-1}) as the feed (Figure 4c), due to more serious membrane fouling
282 and corrosion, the water flux was significantly decreased by ~58.4% at open circuit
283 after 8 h operation. This co-existence of fouling and corrosion also resulted in relatively
284 low salt rejection (but all still higher than 99.8%) due to the enhanced membrane
285 surface wetting from superhydrophobicity to hydrophlicity via more hydrophilic HA
286 accumulation and corrosion-induced surface oxidation during the VMD process (see
287 Figure 5, following section). Significantly improved water flux (14.5 L·m^{-2}·h^{-1}) was
288 observed at -2.0 V for 8 h, much higher (~2.4 times) than that (6.1 L·m^{-2}·h^{-1}) under
289 open circuit. The relatively high salt rejection (above~99.9%) is mainly attributed to
290 membrane wetting inhibition with simultaneously-enhanced anti-corrosion and anti-
291 fouling ability via electrostatic repulsion and electron-supply cathodic protection
292 mechanisms (see Figure 5, following section). The anti-corrosion function under
293 negative polarization is readily confirmed by the result of iron ion content in the
294 oxidized surface per unit membrane area of SS-CNT membrane during 6 h operation
295 (Figure 4d). Compared with the iron ion content (3.1 mg·cm^{-2}) under open circuit, a
296 higher iron ion content (12.5 mg·cm^{-2}) was observed under positive polarization,
297 indicating a significant corrosion. Interesting, a much lower iron ion content (only 0.2
298 mg·cm^{-2}) was obtained under negative polarization due to significantly mitigated
299 corrosion behavior. In addition, compared with spinel-CNT membrane,[17] metal-based
300 SS-CNT membrane exhibited lower resistance and thus higher electrical conductivity
301 (Figure 4e). Moreover, after 6 h operation under negative polarization, the water flux
302 improvement percent of SS-CNT membrane was 2.8 times higher than that of spinel-

CNT membrane, indicating a more promising electrochemically enhanced performance stability (Figure 4f). Therefore, a micro-electrical field-coupling strategy under negative polarization is confirmed to be a highly efficient approach for treatment of high salinity water containing HA, due to enhanced *in situ* anti-fouling and anti-corrosion functions.

Mechanistic Insights into Electrochemically Enhanced Water Treatment

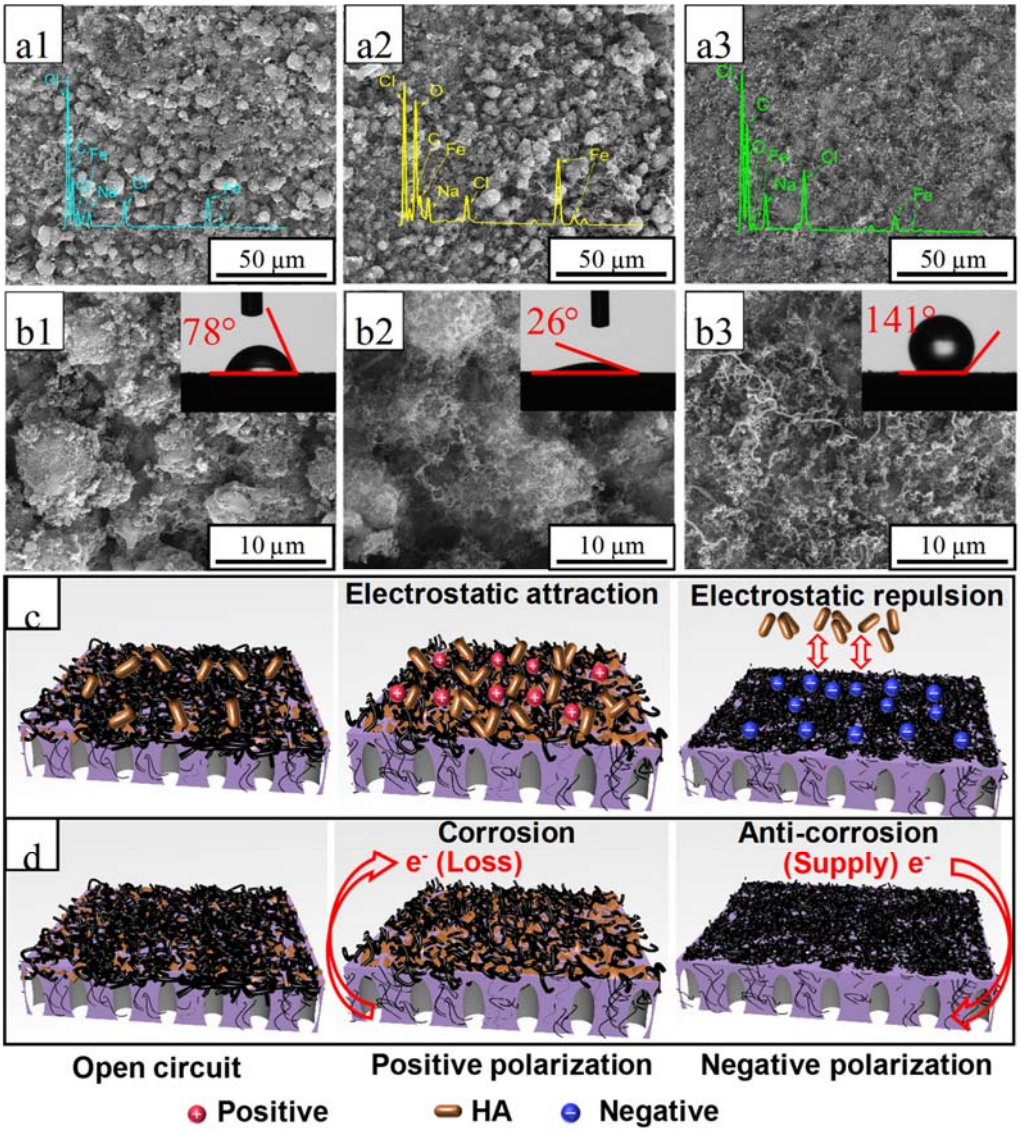

Figure 5. SEM images (a1-a3, b1-b3), EDS spectra (inserted, a1-a3) and water contact angles (inserted, b1-b3) of the SS-CNT membranes for treatment of the organic high salinity feed (70 g·L^{-1} NaCl, 30 mg·L^{-1} HA) after 6 h VMD operation at different electro-chemical conditions: (1) 0 V

313 open circuit, (2) +2.0 V positive polarization, (3) -2.0 V negative polarization. Anti-fouling (c) and
314 anti-corrosion (d) mechanistic models of the SS-CNT membranes under different electrochemically-
315 assisted protocols.

316 Herein, mechanistic insights are provided to understand the simultaneously-
317 enhanced anti-fouling and anti-corrosion performances during VMD of SS-CNT
318 membranes under a micro-electrical field-coupling process. Different alterations in the
319 order of superhydrophobicity-hydrophobicity-hydrophilicity reflect a synergistic effect
320 of membrane fouling and corrosion under different electro-chemical conditions.
321 Inherently, HA is negatively charged and hydrophilic in neutral saline water because of
322 its plentiful oxygen-containing group (such as COO^-) while CNTs are also negatively
323 charged.[49,50] A significant decrease in the water contact angle from 171° (Figure 2d2
324 inset) to 78° (Figure 5b1 inset) was observed after 6 h operation under open circuit,
325 indicating serious membrane fouling-corrosion due to the accumulation of more
326 hydrophilic HA molecules (Figure 5a1). Under positive polarization, however, a highly
327 hydrophilic surface (water contact angle = 26°) of SS-CNT membrane was observed,
328 indicating severe membrane fouling and corrosion. This is the result of an electrostatic
329 attraction, which occurs between positively-charged SS-CNT membrane surface and
330 negatively-charged HA molecules, consequently leading to the accumulation of much
331 more HA on the membrane surface (Figure 5b2 inset). In this case, more severe
332 corrosion was further verified by the EDS analysis (Table S3), which shows a higher
333 Fe content in the form of Fe_2O_3 (Figure 5a2 inset) than in open circuit (Figure 5a1 inset).
334 Under negative polarization, interestingly, membrane fouling was significantly
335 mitigated due to a stronger electrostatic repulsion between the negatively-charged SS-

CNT membrane surface and negatively-charged HA molecules, which is beneficial for treatment of high salinity water containing HA (Figure 5c). This is well verified by a high water contact angle of 141° of the tested SS-CNT membrane after 6 h operation under -2.0 V (Figure 5b3 inset), indicating much less HA coverage on the membrane and that corrosion was significantly mitigated. When the SS-CNT membrane was operated under open circuit, corrosion was observed due to the formation of microcells on the membrane surface in the environments of highly corrosive chloride ion aqueous solutions,[27,51] resulting in a loss of electrons from the SS substrates of SS-CNT membranes. The corrosion was significantly accelerated when the SS-CNT membrane acts as an anode (under positive polarization), due to a much more rapid loss of more electrons from the membrane (Figure 5d). By comparison, when the membrane acts as a cathode under negative polarization, cathodic protection played a key role in anti-corrosion via providing a continuous supply of electrons from Ti anode to SS-CNT membrane (Figure 5d). Therefore, via an enhanced electrostatic repulsion and electron supply mechanism, co-enhancement in anti-fouling and anti-corrosion was simultaneously realized in a negative polarization micro-electrical field-coupling MD process.

IMPLICATIONS

The current study demonstrates that by employing a simple surface activation of Ni and Fe inherently active components, followed by self-catalyzed CVD without external catalyst addition, CNT was functionally constructed *in situ* on flexible high-strength SS substrates via a tip-growth mechanism to form robust superhydrophobic electro-

conductive SS-CNT membranes. A negative polarization micro-electric field strategy coupled with the MD process is demonstrated to simultaneously enhance anti-fouling and anti-corrosion performance for the treatment of organic high-salinity water, which maintains stable flux and solute rejection for a prolonged period of operation. In such a protocol, anti-fouling is realized via enhanced electrostatic repulsion between the membrane surface and humic acid carrying the same negative charges, while anti-corrosion is improved via an electron supply mechanism from Ti anode. Our findings will provide practical guidance for the rational design and fabrication of other metal-based carbon nanotube membranes for electrochemically enhanced wastewater treatment. Inspired by these new phenomena, we can conclude that co-enhancement in anti-fouling and anti-corrosion ability of SS-CNT membrane under negative polarization is expected to be more effective specifically for treating negatively-charged organic wastewater via the MD process. However, for the treatment of positively-charged organic wastewater, anti-corrosion under cathodic protection would be more preferential than anti-fouling for practical applications. Besides demonstrating promising results in the MD application, this electrochemically conducting SS-CNT membrane is also expected to extend toward other potential applications such as membrane evaporation, membrane contactors and membrane adsorption with more interesting electro-chemical functions for the efficient treatment of various emerging organic pollutants such as antibiotics, pharmaceutical and personal care products, and endocrine disrupting compounds in water. To address the issue of thermal conductivity, further studies are needed in the near future for the rational design of both SS-CNT

membranes and membrane modules with more favorable structures to significantly reduce conductive heat transfer in MD. In addition, stainless steel membranes exhibited superior robustness and stability during long-term water filtration process up to 80 h,[26] which appears promising for longer-term desalination durability for practical applications.

ASSOCIATED CONTENT

Supporting Information

S1. Illustration of the preparation and VMD process of SS-CNT membrane (Figure S1); S2. Preparation and characterization of SSHF membrane substrate (Figure S2, Table S1, Figure S3); S3. Properties and cost of SS-CNT membrane (Figure S4, Table S2); S4. TEM and HRTEM images of CNTs (Figure S5); S5. EDS element mapping analysis of oxidized SS-CNT membrane surfaces (Figure S6, Table S3). S6. Evaluation of energy consumption. S7. Performance comparison with other membranes (Table S4).

AUTHOR INFORMATION

Corresponding authors:

Michael D. Guiver (michael.guiver@outlook.com)

Yingchao Dong (ycdong@dlut.edu.cn)

ORCID

1, Michael D. Guiver: 0000-0003-2619-6809

2, Yingchao Dong: 0000-0003-1409-0994

Notes

The authors declare no competing financial interest.

ACKNOWLEDGMENTS

This work was financially supported by the National Natural Science Foundation of China (No. 21876020), Youth Top-Notch Talent Program of Talent Project of Revitalizing Liaoning (No. XLYC1807250), National Key Research and Development Project (No. 2019YFA0705803), Key Project of Liaoning Natural Science Foundation (No. 20180510005), the 111 Program of Introducing Talents of Discipline to Universities (No. B13012), the Haitian Scholar Program from Dalian University of Technology and the project of Changzhou Science and Technology (No. CJ20190013). We also thank Mr. Qifeng Zheng for improving some figure artwork and Dr. Meng Sun (Department of Chemical and Environmental Engineering, Menachem Elimelech group, Yale University) for helpful discussion.

REFERENCES

(1) Shannon, M.; Bohn, P.; Elimelech, M.; Georgiadis, J.; Mariñas, B. J.; Mayes, A. M. Science and technology for water purification in the coming decades. *Nature* **2008**, *452*, (7185), 301-310.

(2) Werber, J. R.; Osuji, C. O.; Elimelech, M. Materials for next-generation desalination and water purification membranes. *Nat. Rev. Mater.* **2016**, *1*, (5), 16018.

(3) Lin, S. Energy Efficiency of Desalination: Fundamental Insights from Intuitive Interpretation. *Environ. Sci. Technol.* **2020**, *54*, (1), 76-84.

(4) Kezia, K.; Lee, J.; Weeks, M.; Kentish, S. Direct contact membrane distillation for the concentration of saline dairy effluent. *Water Res.* **2015**, *81*, 167-177.

(5) Tong, T.; Elimelech, M. The global rise of zero liquid discharge for wastewater management: drivers, technologies, and future directions. *Environ. Sci. Technol.* **2016**, *50*, (13), 6846-6855.

(6) Kim, J. H.; Park, S. H.; Lee, M. J.; Lee, S. M.; Lee, W. H.; Lee, K. H.; Kang, N. R.; Jo, H. J.; Kim, J. F.; Drioli, E. Thermally rearranged polymer membranes for desalination. *Energy Environ. Sci.* **2016**, *9*, (3), 878-884.

(7) Wang, Z.; Lin, S. Membrane fouling and wetting in membrane distillation and their mitigation

by novel membranes with special wettability. *Water Res.* **2017**, *112*, 38-47.

(8) Rezaei, M.; Warsinger, D. M.; Duke, M. C.; Matsuura, T.; Samhaber, W. M. Wetting phenomena in membrane distillation: mechanisms, reversal, and prevention. *Water Res.* **2018**, *139*, 329-352.

(9) Straub, A. P.; Yip, N. Y.; Lin, S.; Lee, J.; Elimelech, M. Harvesting low-grade heat energy using thermo-osmotic vapour transport through nanoporous membranes. *Nat. Energy* **2016**, *1*, (7), 16090.

(10) Dongare, P. D.; Alabastri, A.; Pedersen, S.; Zodrow, K. R.; Hogan, N. J.; Neumann, O.; Wu, J.; Wang, T.; Deshmukh, A.; Elimelech, M. Nanophotonics-enabled solar membrane distillation for off-grid water purification. *Proc. Natl. Acad. Sci. U.S.A.* **2017**, *114*, (27), 6936-6941.

(11) Dudchenko, A. V.; Chen, C.; Cardenas, A.; Rolf, J.; Jassby, D. Frequency-dependent stability of CNT Joule heaters in ionizable media and desalination processes. *Nat. Nanotechnol.* **2017**, *12*, (6), 557.

(12) Cerneaux, S.; Strużyńska, I.; Kujawski, W. M.; Persin, M.; Larbot, A. Comparison of various membrane distillation methods for desalination using hydrophobic ceramic membranes. *J. Membr. Sci.* **2009**, *337*, (1-2), 55-60.

(13) Liu, F.; Hashim, N. A.; Liu, Y.; Abed, M. M.; Li, K. Progress in the production and modification of PVDF membranes. *J. Membr. Sci.* **2011**, *375*, (1-2), 1-27.

(14) Drioli, E.; Ali, A.; Macedonio, F. Membrane distillation: Recent developments and perspectives. *Desalination* **2015**, *356*, 56-84.

(15) Huang, Y.-X.; Wang, Z.; Jin, J.; Lin, S. Novel Janus membrane for membrane distillation with simultaneous fouling and wetting resistance. *Environ. Sci. Technol.* **2017**, *51*, (22), 13304-13310.

(16) Deshmukh, A.; Boo, C.; Karanikola, V.; Lin, S.; Straub, A. P.; Tong, T.; Warsinger, D. M.; Elimelech, M. Membrane distillation at the water-energy nexus: limits, opportunities, and challenges. *Energy Environ. Sci.* **2018**, *11*, (5), 1177-1196.

(17) Dong, Y.; Ma, L.; Tang, C. Y.; Yang, F.; Quan, X.; Jassby, D.; Zaworotko, M. J.; Guiver, M. D. Stable superhydrophobic ceramic-based carbon nanotube composite desalination membranes. *Nano Lett.* **2018**, *18*, (9), 5514-5521.

(18) Zhang, H.; Li, B.; Sun, D.; Miao, X.; Gu, Y. SiO_2-PDMS-PVDF hollow fiber membrane with high flux for vacuum membrane distillation. *Desalination* **2018**, 429, 33-43.

(19) Ardeshiri, F.; Salehi, S.; Peyravi, M.; Jahanshahi, M.; Amiri, A.; Rad, A. S. PVDF membrane assisted by modified hydrophobic ZnO nanoparticle for membrane distillation. *Asia-Pac. J. Chem. Eng.* **2018**, *13*, (3), e2196.

(20) Kujawa, J.; Cerneaux, S.; Koter, S.; Kujawski, W. Highly efficient hydrophobic titania ceramic membranes for water desalination. *ACS Appl. Mater. Interfaces* **2014**, *6*, (16), 14223-14230.

(21) Liu, T.; Lei, L.; Gu, J.; Wang, Y.; Winnubst, L.; Chen, C.; Ye, C.; Chen, F. Enhanced water desalination performance through hierarchically-structured ceramic membranes. *J. Eur. Ceram. Soc.* **2017**, *37*, (6), 2431-2438.

(22) Chen, X.; Gao, X.; Fu, K.; Qiu, M.; Xiong, F.; Ding, D.; Cui, Z.; Wang, Z.; Fan, Y.; Drioli, E. Tubular hydrophobic ceramic membrane with asymmetric structure for water desalination via vacuum membrane distillation process. *Desalination* **2018**, *443*, 212-220.

(23) Zhang, M.; Jin, W.; Yang, F.; Duke, M.; Dong, Y.; Tang, C. Y. Engineering a Nanocomposite Interlayer for a Novel Ceramic-Based Forward Osmosis Membrane with Enhanced Performance. Environmental Science & Technology 2020. DOI: 10.1021/acs.est.0c02809.

(24) Yuan, Z.; Yu, Y.; Wei, L.; Sui, X.; She, Q.; Chen, Y., Pressure-retarded membrane distillation for simultaneous hypersaline brine desalination and low-grade heat harvesting. *J. Membr. Sci.* **2020**, 597, 117765.

(25) Chong, J. Y.; Wang, B.; Li, K. High performance stainless steel-ceramic composite hollow fibres for microfiltration. *J. Membr. Sci.* **2017**, *541*, 425-433.

(26) Wang, M.; Cao, Y.; Xu, Z.-L.; Li, Y.-X.; Xue, S.-M. Facile fabrication and application of superhydrophilic stainless steel hollow fiber microfiltration membranes. *ACS Sustain. Chem. Eng.* **2017**, *5*, (11), 10283-10289.

(27) Cui, Y.; Liu, S.; Smith, K.; Yu, K.; Hu, H.; Jiang, W.; Li, Y. Characterization of corrosion scale formed on stainless steel delivery pipe for reclaimed water treatment. *Water Res.* **2016**, *88*, 816-825.

(28) Chen, M.; Zhu, L.; Chen, J.; Yang, F.; Tang, C. Y.; Guiver, M. D.; Dong, Y. Spinel-based ceramic membranes coupling solid sludge recycling with oily wastewater treatment. *Water Res.* **2020**, *169*, 115180.

(29) Wang, X.; Li, Y.; Yu, H.; Yang, F.; Tang, C. Y.; Quan, X.; Dong, Y. High-flux robust ceramic membranes functionally decorated with nano-catalyst for emerging micro-pollutant removal from water. J. Membr. Sci. 2020, 118281. Doi: 10.1016/j.memsci.2020.118281.

(30) Luiten-Olieman, M. W.; Winnubst, L.; Nijmeijer, A.; Wessling, M.; Benes, N. E. Porous stainless steel hollow fiber membranes via dry–wet spinning. *J. Membr. Sci.* **2011**, *370*, (1-2), 124-

130.

(31) Rui, W.; Zhang, C.; Cai, C.; Gu, X. Effects of sintering atmospheres on properties of stainless steel porous hollow fiber membranes. *J. Membr. Sci.* **2015**, *489*, 90-97.

(32) Michielsen, B.; Chen, H.; Jacobs, M.; Middelkoop, V.; Mullens, S.; Thijs, I.; Buekenhoudt, A.; Snijkers, F. Preparation of porous stainless steel hollow fibers by robotic fiber deposition. *J. Membr. Sci.* **2013**, *437*, 17-24.

(33) Liu, S.; Li, K. Preparation TiO_2/Al_2O_3 composite hollow fibre membranes. *J. Membr. Sci.* **2003**, *218*, (1-2), 269-277.

(34) Zhang, X.; Lin, B.; Ling, Y.; Dong, Y.; Fang, D.; Meng, G.; Liu, X. Highly permeable porous YSZ hollow fiber membrane prepared using ethanol as external coagulant. *J. Alloy. Compd.* **2010**, *494*, (1-2), 366-371.

(35) de Wit, P.; Kappert, E. J.; Lohaus, T.; Wessling, M.; Nijmeijer, A.; Benes, N. E. Highly permeable and mechanically robust silicon carbide hollow fiber membranes. *J. Membr. Sci.* **2015**, *475*, 480-487.

(36) Zhang, J.-W.; Fang, H.; Wang, J.-W.; Hao, L.-Y.; Xu, X.; Chen, C.-S. Preparation and characterization of silicon nitride hollow fiber membranes for seawater desalination. *J. Membr. Sci.* **2014**, *450*, 197-206.

(37) Zhu, L.; Chen, M.; Dong, Y.; Tang, C. Y.; Huang, A.; Li, L. A low-cost mullite-titania composite ceramic hollow fiber microfiltration membrane for highly efficient separation of oil-in-water emulsion. *Water Res.* **2016**, *90*, 277-285.

(38) Tai, Z. S., Abd Aziz, M. H., Othman, M. H. D., Mohamed Dzahir, M. I. H., Hashim, N. A., Koo, K. N., Jaafar, J. Ceramic Membrane Distillation for Desalination. *Sep. Purif. Rev.* **2019**, 1–40.

(39) Chen, M.; Zhu, L.; Dong, Y.; Li, L.; Liu, J., Waste-to-Resource Strategy To Fabricate Highly Porous Whisker-Structured Mullite Ceramic Membrane for Simulated Oil-in-Water Emulsion Wastewater Treatment. *ACS Sustain. Chem. Eng.* **2016**, *4*, (4), 2098-2106.

(40) Camilli, L.; Scarselli, M.; Del Gobbo, S.; Castrucci, P.; Nanni, F.; Gautron, E.; Lefrant, S.; De Crescenzi, M. The synthesis and characterization of carbon nanotubes grown by chemical vapor deposition using a stainless steel catalyst. *Carbon* **2011**, *49*, (10), 3307-3315.

(41) Zhuo, C.; Wang, X.; Nowak, W.; Levendis, Y. A. Oxidative heat treatment of 316L stainless steel for effective catalytic growth of carbon nanotubes. *Appl. Surf. Sci.* **2014**, *313*, 227-236.

(42) Liao, Y.; Loh, C.-H.; Wang, R.; Fane, A. G. Electrospun superhydrophobic membranes with unique structures for membrane distillation. *ACS Appl. Mater. Interfaces* **2014**, *6*, (18), 16035-16048.

(43) Zhang, D.; Ye, K.; Yao, Y.; Liang, F.; Qu, T.; Ma, W.; Yang, B.; Dai, Y.; Watanabe, T. Controllable synthesis of carbon nanomaterials by direct current arc discharge from the inner wall of the chamber. *Carbon* **2019**, *142*, 278-284.

(44) Sano, N.; Yamamoto, S.; Tamon, H. Cr as a key factor for direct synthesis of multi-walled carbon nanotubes on industrial alloys. *Chem. Eng. J.* **2014**, *242*, 278-284.

(45) Vander Wal, R. L.; Hall, L. J. Carbon nanotube synthesis upon stainless steel meshes. *Carbon* **2003**, *41*, (4), 659-672.

(46) Ashraf, A.; Salih, H.; Nam, S.; Dastgheib, S. A. Robust carbon nanotube membranes directly grown on Hastelloy substrates and their potential application for membrane distillation. *Carbon* **2016**, *106*, 243-251.

(47) Hashempour, M.; Vicenzo, A.; Zhao, F.; Bestetti, M. Direct growth of MWCNTs on 316 stainless steel by chemical vapor deposition: Effect of surface nano-features on CNT growth and structure. *Carbon* **2013**, *63*, 330-347.

(48) Zhu, L.; Dong, X.; Xu, M.; Yang, F.; Guiver, M. D.; Dong, Y. Fabrication of mullite ceramic-supported carbon nanotube composite membranes with enhanced performance in direct separation of high-temperature emulsified oil droplets. *J. Membr. Sci.* **2019**, *582*, 140-150.

(49) Yuan, W.; Zydney, A. L. Humic acid fouling during ultrafiltration. *Environ. Sci. Technol.* **2000**, *34*, (23), 5043-5050.

(50) Wang, J.; Liu, P.; Xia, B.; Wei, H.; Wei, Y.; Wu, Y.; Liu, K.; Zhang, L.; Wang, J.; Li, Q. Observation of charge generation and transfer during CVD growth of carbon nanotubes. *Nano Lett.* **2016**, *16*, (7), 4102-4109.

(51) Poursaee, A.; Laurent, A.; Hansson, C. Corrosion of steel bars in OPC mortar exposed to NaCl, $MgCl_2$ and $CaCl_2$: Macro-and micro-cell corrosion perspective. *Cement Concrete Res.* **2010**, *40*, (3), 426-430.